Equilibrium Statistics of a Surface-Pinned Semiflexible Polymer

ARTICLE *in* MACROMOLECULES · JANUARY 2013

Impact Factor: 5.8 · DOI: 10.1021/ma4011704

2 AUTHORS, INCLUDING:

Harold D Kim
Georgia Institute of Technology
32 PUBLICATIONS **1,931** CITATIONS

SEE PROFILE

Macromolecules

Article

pubs.acs.org/Macromolecules

Equilibrium Statistics of a Surface-Pinned Semiflexible Polymer

James T. Waters and Harold D. Kim*

School of Physics, Georgia Institute of Technology, Atlanta, Georgia 30332, United States

Supporting Information

ABSTRACT: Recently, looping probability of short double-stranded DNA (dsDNA) was measured from surface-tethered molecules and was shown to exceed the wormlike chain model prediction. However, it is not clear how the presence of a confining surface affects the structure of the polymer. Here, we investigate the conformational distribution of an isolated, surface-pinned dsDNA in the semiflexible regime. To obtain chain statistics, we randomly sampled chain conformations consistent with Boltzmann statistics and the confining surface. On the basis of comparison of simulated chain statistics to a theoretical wormlike chain model, we show that the effect of pinning can be analogous to a change in effective stiffness. In the semiflexible regime, middle pinning results in a 10-fold increase in looping probability and 100-fold increase in surface contact rate compared to end pinning. Our results highlight nontrivial effects of pinning a wormlike chain that cannot be deduced from the Gaussian chain model.

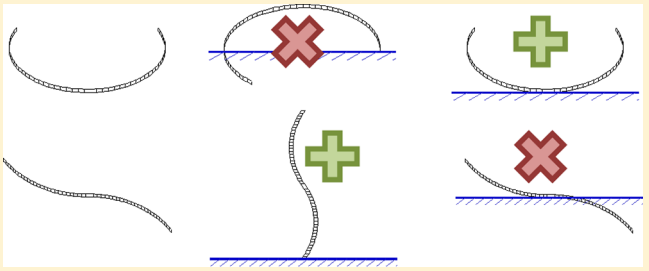

INTRODUCTION

Ideal chain models can provide useful insights into dynamics of polymers, but a real polymer experiences additional complex interactions: self-interaction between its monomers, interaction with other polymers, and interaction with the boundaries of its environment. Understanding how these factors affect polymer dynamics is one of the main goals of polymer physics. Some effects can be incorporated in the form of simple scaling laws or more complex models. For example, the excluded volume interaction between monomers can be described by the Flory radius,[1,2] and finite bending energy between adjacent monomers can be described by the wormlike chain model.[3]

In many circumstances and applications in industry and medicine, polymers are adsorbed onto interfaces, and therefore, conformation of adsorbed polymers has been a subject of intensive study. Although a great body of work initially began on the conformation of an isolated polymer,[4−7] this soon gave way to studies of polymer layers because properties of a single polymer were not experimentally accessible at the time.[8−12] With the advent of single molecule techniques, it has now become possible to test some aspects of a polymer model with an isolated, surface-tethered macromolecule.

In general, confinement geometry modifies the size, shape, and dynamics of polymer chains.[13] For some cases, the effect of the surface on the conformation of a single chain can be understood theoretically. A Gaussian chain (or a flexible chain) end-grafted to a surface is one good example. Using the reflection theorem, one can show that the end-to-end distance probability distribution changes from a Gaussian function to its derivative.[14−16] As a result, the mean-square end-to-end distance along the confined dimension is increased by a factor of 2. Additionally, the number of available conformations is reduced by a factor proportional to the square root of the chain size. Unlike a flexible chain, the end-to-end distance probability distribution of a semiflexible chain pinned to a hard wall cannot be derived analytically. Hence, previous efforts adopted Metropolis Monte Carlo methods to simulate chain conformations compatible with the given physical constraints.[17,18]

Here, we investigate the equilibrium statistics of a surface-pinned wormlike chain. In a wormlike chain, energy is associated with the bending angle between adjacent monomers, and therefore simple random walk statistics do not apply. On the other hand, because self-intersecting conformations are rare in the semiflexible regime where the contour length is on the order of the persistence length,[19] the probability of each chain conformation depends only on the bending energy through the Boltzmann factor with no preferred kinetic trajectory. Therefore, we use a Gaussian sampling method[20−22] which is computationally lighter than Monte Carlo methods to study the effect of surface-pinning.

This study is also motivated by recent experiments that tried to test the wormlike chain model on short dsDNA molecules.[22,23] In these studies, dsDNA was tethered to a surface, and its looping behavior was observed by single-molecule fluorescence resonance energy transfer (smFRET). The looping probability density known as the J factor was measured to be higher than the wormlike chain model prediction, confirming the results of previous studies.[24−26] However, since the molecules were confined to the half space, it remains questionable whether it is valid to use the J factor derived for the free chain to test the wormlike chain model. While the fraction of looped conformations is low, it is

Received: June 6, 2013
Revised: July 24, 2013
Published: August 14, 2013

   dx.doi.org/10.1021/ma4011704 | Macromolecules 2013, 46, 6659−6666

determined by the chain statistics over the entire range of end-to-end distances. Hence, we compare the chain statistics between an unconstrained chain and a surface-pinned chain and show how chain statistics are altered depending on pinning position. To characterize the pinning effect in terms of effective stiffness, we fit the end-to-end distance distribution of a free chain to the simulated distribution. Depending on the pinning position, effective stiffness can be increased by up to 8% or decreased by over 25%. The rejection rate of a middle-pinned chain is 100-fold higher and also exhibits opposite temperature dependence compared to an end-pinned chain. This work provides a useful guideline for the design and analysis of experiments on surface-tethered polymers at small length scales.

MATERIALS AND METHODS

Notation Convention. The free chain statistics are characterized by stiffness $\kappa = L_p/L$, where L and L_p are the contour length and the persistence length of the chain, respectively. The persistence length of dsDNA is taken to be 146 bp consistent with MD simulation.[27] For simplicity, we treated the DNA chain as electrostatically neutral, which is a reasonable assumption based on the short Debye screening length (0.8 nm) in physiological salt conditions ($[Na^+]$ = 150 mM). In principle, salt effectively decreases the persistence length[28,29] but only by ~4% between 100 mM and 1 M $[Na^+]$.[30] r is the end-to-end distance scaled by L and is also called the extension ($0 \le r \le 1$). For clarity throughout the paper and consistency with the literature,[31] we define two distribution functions (or probability densities): probability distribution function of end-to-end distance $Q(r)$ and radial distribution function $4\pi r^2 Q(r)$. By this definition, it is the radial distribution function that is normalized.

Gaussian Sampling of Dinucleotide Chain Conformations. We implemented the rigid base-pair model to build discrete conformations of a wormlike chain.[22,32] The model considers three dinucleotide angles known as roll (ρ), tilt (τ), and twist (Ω) to define the orientation of the next base pair with respect to the current one.[33] We assumed an intrinsically straight dsDNA molecule with uniform, isotropic bending fluctuations. The bending fluctuations were adjusted so that they produce the same overall bending and twisting persistence lengths as the molecular dynamics simulation performed with CHARMM27 force field.[34] Roll and tilt fluctuations are both equal to 4.7°, and the twist fluctuation is 4.1° at 20 °C. We used a Gaussian sampling method[20,21] to generate DNA conformations in thermal equilibrium. Numbers were sampled from the standard normal distribution and scaled according to their respective bending fluctuation parameters to yield dinucleotide angles. The tangent vectors ($\mathbf{d}_i$) were then obtained by rolling, tilting, and twisting a unit vector based on these angles by matrix multiplication:

$$\mathbf{d}_i = \mathbf{G}_{0,1}\mathbf{G}_{1,2}\cdots\mathbf{G}_{i-1,i}\mathbf{d}_0$$

where the matrix $\mathbf{G}$ transforms between the coordinate frames of adjacent monomers

$$\mathbf{G} = \begin{pmatrix} \cos\rho\cos\Omega - \sin\tau\sin\rho\sin\Omega & -\cos\tau\sin\Omega & \sin\rho\cos\Omega + \sin\tau\cos\rho\sin\Omega \\ \cos\rho\sin\Omega + \sin\tau\sin\rho\cos\Omega & \cos\tau\cos\Omega & \sin\rho\sin\Omega - \sin\tau\cos\rho\cos\Omega \\ -\cos\tau\sin\rho & \sin\tau & \cos\tau\cos\rho \end{pmatrix} \quad (1)$$

We used C++ on a Windows PC to perform this calculation. For free chains of one persistence length, it normally takes 600 s to generate 10^7 chains. This running time scales linearly with both the length of the chains and the number of chains generated.

Rejection Criterion. For free chains, the orientation of the chain in space is irrelevant for computing $Q(r)$. However, this is not the case when the chain is pinned to a surface. To account for the fact that some fraction of orientations will result in the chain intersecting the bounding surface, the chain will be given a random rotation from some known orientation. The probability that the conformation will be accepted will be proportional to the fraction of possible orientations such that the chain does not intersect the surface.

We define the xy plane to be the bounding surface. Initially, the first monomer of the chain linked to the surface is (0, 0, 1). The orientation of the chain is then randomized by rotating the chain by an angle ϕ about the z-axis and θ about the x-axis. The angle ϕ is chosen uniformly over the interval $0 \le \phi < 2\pi$. All values of $\theta > \pi/2$ result in a chain that crosses the boundary; therefore, θ was restricted to the range $0 \le \theta \le \pi/2$. To compensate for this restriction, an additional rejection was counted for both every rejected and accepted chain. By choosing θ with probability proportional to $\sin\theta$, we generate a distribution of θ and φ corresponding to points evenly distributed over the surface of the $z \ge 0$ hemisphere.

When the chains are pinned internally, it is more efficient to begin building conformations from one of the pinned monomers at a random orientation. Other links of the chain can be computed both forward and backward from this point ($\mathbf{d}_m$). Links forward of the pinning position can be generated as before

$$\mathbf{d}_n = \mathbf{G}_{m,m+1}\mathbf{G}_{m+1,m+2}\cdots\mathbf{G}_{n-1,n}\mathbf{d}_m$$

and links prior to the pinning position can be computed as

$$\mathbf{d}_l = \mathbf{G}^{-1}_{m-1,m}\mathbf{G}^{-1}_{m-2,m-1}\cdots\mathbf{G}^{-1}_{l,l+1}\mathbf{d}_m$$

As links are added to the chain, the coordinates of the ends of the chain can be updated in a running tally of the displacement vectors starting from the pinning point. If this displacement vector crosses the boundary, we can reject the conformation without proceeding any further. New random angles are generated, the count of rejected chains is incremented, and the process begins again. If no boundary crossing has occurred after the entire chain has been generated, the chain is accepted and the end-to-end distance is recorded.

Implementing other types of boundaries, such as a spherical shell geometry, can be done by changing the rejection criterion. The algorithm proceeds as before, but instead of using the surface $z = 0$, we substitute a different surface function $z(x,y)$.

Simulation of $Q(r)$. We continued the simulation until 10^7 chains were accepted. We plotted the histogram of end-to-end distances using a bin width equal to one helical rise (1 bp) and normalized it by the total number of chains. Hence, the amplitude in each bin corresponds approximately to $4\pi r^2 Q(r)\Delta r$ because the bin width ($\Delta r = 1/L$) is much smaller than 1. $Q(r)$ can thus be obtained by dividing the histogram amplitude by $4\pi r^2 \Delta r$.

Calculation of $Q(r)$ for an Unconstrained Semiflexible Chain. The Fourier transform of the end-to-end distance probability density for the free chain can be found by modeling the tangent vector at each link as a particle diffusing on the unit sphere.[35] The resulting path integral can be solved in Fourier−Laplace space to give a solution that can be conveniently expressed as an infinite continued fraction according to Mehraeen et al.[36] The Laplace transform of the Fourier transform $\hat{Q}$ is given by

$$(\mathcal{L}\hat{Q})(p, K) = \cfrac{1}{P_0 + \cfrac{(a_1K)^2}{P_1 + \cfrac{(a_2K)^2}{P_2 + \cdots}}} \quad (2)$$

where $P_{n=0,1,2\ldots}$ and $a_{n=1,2,3\ldots}$ are defined as $P_n = p + n(n+1)$ and $a_n = n/(4n^2-1)^{1/2}$. K is the reduced Fourier variable conjugate to the end-to-

dx.doi.org/10.1021/ma4011704 | Macromolecules 2013, 46, 6659−6666

end distance (r), and p is the Laplace conjugate of the number of statistical segments (N). The partial summation $P_n + (a_{n+1}k)^2/P_{n+1} + ...$ is denoted by j_n.

To efficiently invert both transforms, we followed the procedure given by Mehraeen et al.[36] The Laplace transform is inverted by identifying the poles ε_l of the expression in eq 2 and employing the residue theorem.

$$\hat{Q}(K) = \sum_{l=0}^{\infty} \frac{\exp(\varepsilon_l N)}{\partial_p j_0(K, \varepsilon_l)} \tag{3}$$

The poles ε_l correspond to the eigenvalues of the symmetric tridiagonal matrix $-\mathbf{J}^{(0)}$, specified by diagonal entries $\mathbf{J}^{(0)}_{n,n} = n(n+1)$ and off-diagonal entries $\mathbf{J}^{(0)}_{n+1,n} = -ia_nK$, with a_n defined as above. The infinite matrix is truncated at some size n_{cutoff}, which will give eigenvalues ε_n up to $n = n_{\text{cutoff}}/4$ with sufficient accuracy.

The derivative of j_0 can be computed using a recursive relation

$$\partial_p j_n^{(+)} = 1 - \frac{(a_{n+1}K)^2}{j_{n+1}^{(+)2}} \partial_p j_{n+1}^{(+)} \tag{4}$$

beginning with some $\partial_p j_{n_{\text{cutoff}}} = 1$ and $j_{n_{\text{cutoff}}} = P_{n_{\text{cutoff}}}$. After evaluating the above over a range of wavenumbers K, it is converted into a density in real space by inverting the Fourier transform

$$Q(r) = \frac{1}{(2L_p)^3} \frac{1}{2\pi^2} \int_0^{\infty} K^2 \frac{\sin(NrK)}{NrK} \hat{Q}(K)\, dK \tag{5}$$

using numerical quadrature.

RESULTS AND DISCUSSION

Difference in Looping Fraction. In the presence of a boundary, direct computation of the radial distribution function of a pinned wormlike chain is intractable. Therefore, we performed computer simulation to build an ensemble of chain conformations compatible with the confining surface (Figure 1A). We used 186-bp long dsDNA as the model polymer and applied the rigid base-pair model to generate conformations.[22] The looping fraction is defined as the fraction of conformations whose end-to-end distances lie within some trapping radius (r_c) of 10 bp which corresponds to ~0.05 for this length. The results in Figure 1B show the effect of the surface on the looping fraction of a chain with stiffness $\kappa = 0.78$. For terminally pinned chains or chains pinned internally near the end, the surface decreases the looping rate by approximately half relative to the free chain. A similar refractory effect of bounding surfaces on looping was shown in previous studies.[18,21] When the chain is pinned near the middle, however, the surface has the effect of increasing the looping rate by a factor of 5, which does not change significantly in the semiflexible regime (see Supporting Information). This difference decreases at larger lengths. Mathematically, the looping fraction is equal to the end-to-end probability distribution $Q(r)$ integrated over the spherical volume of radius r_c. The J factor, which is the most widely used quantity to describe flexibility of dsDNA,[37] is equivalent to $\lim_{r\to 0} Q(r)$ in molar units. In the case that $r_c \ll 1$, the J factor is thus proportional to the looping fraction. This result shows that the J factor derived for a free chain[38−40] needs to be corrected when applied to surface-tethered polymers.[22,23]

The 5-fold difference in looping fraction between the free and middle-pinned geometries highlights the semiflexible behavior as it is significantly higher than would be expected for a Gaussian chain. Using the reflection principle[14] to obtain end-to-end distance distributions for pinned and free cases, we can compute the expected ratio of the middle-pinned looping fraction relative to that of the free chain, which approaches $\pi/2$. No similar result exists for Gaussian chains in the end-pinned geometry, as the looping fraction falls off more quickly with the number of statistical segments (N) than it does for either the middle-pinned or free geometry, by a factor of $N^{1/2}$. As a consequence, in the limit of long chains the ratio of looping fractions approaches zero.

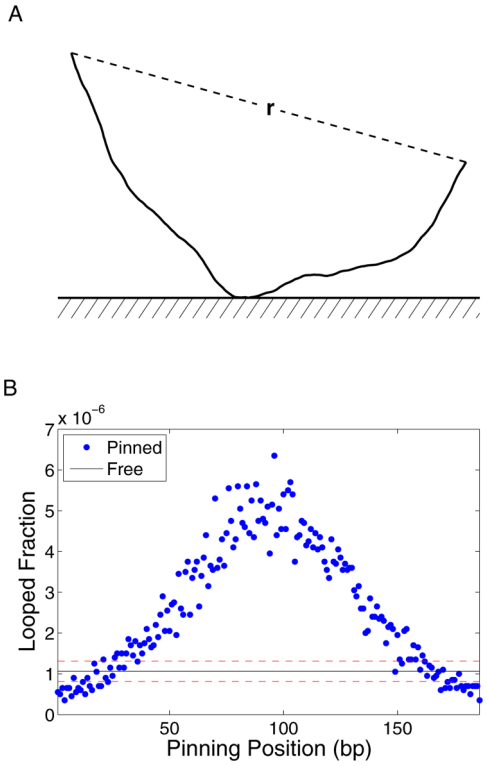

Figure 1. (A) The experimental setup we are trying to simulate. The DNA chain is pinned to the surface at an arbitrary position, which will limit its conformational space and affect the distribution of end-to-end distances. (B) The measured looping fraction as a function of pinning position, for a 186-bp chain. When pinned near the end, the surface excludes looped conformations more often than unlooped conformations, and the looped fraction is decreased relative to the free chain. When pinned closer to the middle, unlooped conformations are rejected at a greater rate and so the looped fraction increases. For comparison, the looping fraction of a free chain is indicated by the solid horizontal line with the dashed lines representing 95% confidence intervals.

Difference in End-to-End Distance Probability Distribution. Knowing that the looping fraction of surface-pinned chains deviates from that of a free chain, we asked how $Q(r)$ changes with the pinning position. We focused on two extreme pinning positions: end-pinned and middle-pinned. $Q(r)$ for free, end-pinned, and middle-pinned chains are shown in Figure 2 for comparison. For the 186-bp chains we considered, the middle-pinned chain has the highest probability density below the extension of 0.8, whereas the end-pinned chain has the highest above 0.8. The reason for this difference in the surface effect is because different conformations are accepted or rejected at different rates depending on where the chain is pinned. Intuitively, end-pinned chains are accepted at a higher rate at long end-to-end distances than at short end-to-end distances. In contrast, the acceptance rate for middle-pinned chains is lowest at large end-to-end distances, increasing as the end-to-end distance decreases. This causes $Q(r)$ for the end-

dx.doi.org/10.1021/ma4011704 | Macromolecules 2013, 46, 6659−6666

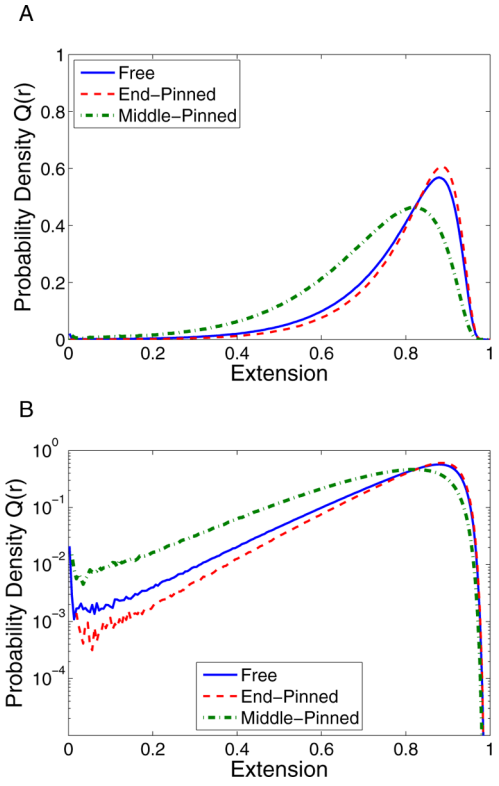

Figure 2. (A) Probability density of end-to-end distances for 186-bp chains in different pinning schemes. Relative to the free case (solid line), the end-pinned chain (dashed line) favors longer extensions, while the middle-pinned chain (dot-dashed line) favors shorter extensions. (B) The same data on a log scale. This better displays the significant change in probability density at small extensions for end- and middle-pinned chains.

pinned system to skew toward larger distances and $Q(r)$ for the middle-pinned system to skew toward shorter distances compared to that of the free chain. We note that $Q(r)$ of a Gaussian chain changes dramatically due to pinning. For example, $Q(0)$ of a free Gaussian chain would change from peak to zero as a result of end pinning. A wormlike chain thus undergoes a much smaller change in $Q(r)$ than a Gaussian chain as a result of surface pinning.

Acceptance Rate for Surface-Pinned Chains. To better understand the origin of skewing of $Q(r)$, we calculated the fraction of chains that are accepted in each pinning scheme, which we term the acceptance rate (A). Although we treat the surface as a hard wall for simplicity, the surface effect in experimental settings would be much more complicated. Regardless of the details of the surface effects, the rejection rate ($1 - A$) might serve as a measure of the frequency of contact between the chain and the surface. Since we reject chains on their first contact with the surface, the actual contact frequency is expected to be higher. For a flexible chain, the fraction of conformations that do not cross the boundary is expected to scale with length as $L^{-0.5}$,[14,16] which is consistent with our measured scaling of $A \propto L^{-0.49}$ at large length scales. The acceptance rate for middle-pinned chains scales as $A \propto L^{-0.96}$, which is approximately the square of the power law found for the end-pinned chains. This is the result we would expect, as there are two halves of the chain extending from the pinning position, both obeying the $L^{-0.5}$ power law. At short length scales, the acceptance rate for the middle-pinned chain scales as $A \propto L^{-0.52}$, while the terminally pinned chains do not obey any clear power law. Near 100-bp in the semiflexible regime, the acceptance rate of a middle-pinned chain (0.002) was about 200-fold lower than that of an end-pinned chain (0.4). This gap in the acceptance rate reflects the bending energy penalty associated with the internally pinned dimer. Without this, the acceptance rate of the middle-pinned chain would be simply the square of the acceptance rate of an end-pinned chain with half the length ($0.4^2 = 0.16$). This result suggests that a middle-pinned wormlike chain would undergo surface contacts at least 2 orders of magnitude more frequently than an end-pinned counterpart.

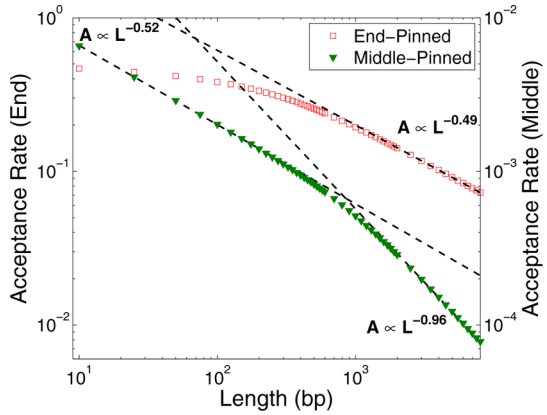

Figure 3. Acceptance rate (A) versus length. The end-pinned chain approaches an acceptance rate of 50% for short lengths, which we would expect for a perfectly straight rod. At long lengths, it obeys a power law $A \propto L^{-0.49}$. The acceptance rate for middle-pinned chain goes as $A \propto L^{-0.52}$ at short length scales and as $A \propto L^{-0.96}$. Note that the two curves are on different scales, as the acceptance rate for middle-pinned chains is significantly lower at all length scales.

The acceptance rate is also equal to the fraction of conformational space available to a pinned chain compared to a free chain and is thus related to the entropy difference between the bound and unbound states. The middle-pinned chain gains more entropy by escaping from the surface than the end-pinned chain[41] and, therefore, would be more unstable. This difference in stability of the bound state could be measured experimentally by the difference in the rate of dissociation from the surface.

Effect of Surface Pinning on Apparent Stiffness. We then asked whether the skewed distributions could correspond to a distribution of an unconstrained wormlike chain of arbitrary stiffness. The end-to-end distance or radial density function for unconstrained wormlike chains has been extensively studied and can be approximated in many different forms.[19,39,42−44] However, these approximations are tailored for particular ranges of extensions and flexibility regimes as shown by Becker et al.[31] Because we are trying to identify an unknown stiffness parameter that best represents the distribution over the entire extension range, we numerically evaluated the exact solution as a function of stiffness.[35,36] The stiffness paramter was obtained by minimizing the sum of squared residuals between the simulated and calculated distributions. As shown in the left panel of Figure 4, the simulated distribution of a free dsDNA closely matches the calculated distribution of a wormlike chain, which confirms the validity of our simulation. The best-fit value for the intrinsic stiffness ($\kappa = 0.78$) for a 186-

dx.doi.org/10.1021/ma4011704 | Macromolecules 2013, 46, 6659−6666

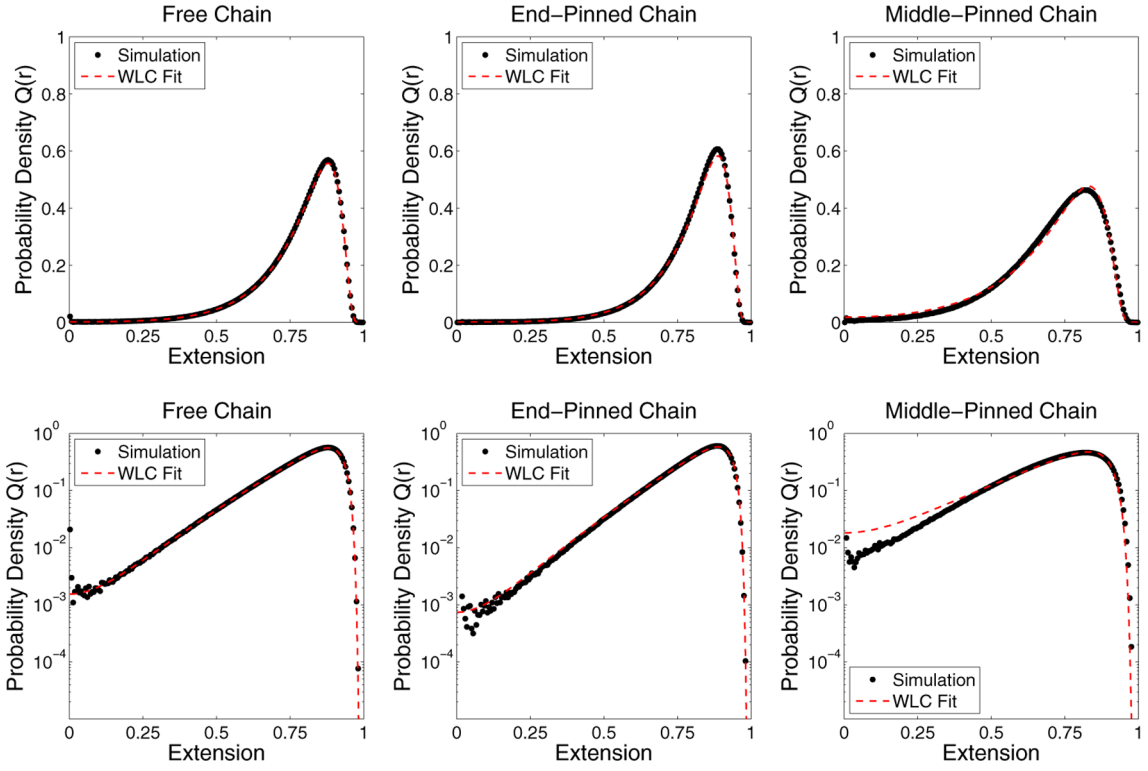

Figure 4. Fits from worm-like chain theory to simulation data for 186-bp chains on linear (top row) and log (bottom row) scales. The end-pinned chains behave like a stiffer free chain, while the middle-pinned chains behave like a more flexible one. Note that the agreement between the fit and the data breaks down at short extensions for the middle-pinned chain (right panel).

bp chain corresponds to a persistence length of 146 bp, which is in agreement with the input bending fluctuations. Fitting this same functional form to the distribution for an end-pinned chain yields a larger stiffness (κ = 0.84) corresponding to a persistence length of 157 bp, while fitting to the middle-pinned chain yields a smaller stiffness (κ = 0.57) which corresponds to a persistence length of 106 bp. This result suggests that an end-pinned chain is statistically similar to a stiffer free chain, and a middle-pinned chain behaves like a more flexible one. For example, compared to a free chain, a middle-pinned chain has an increased probability density at short extensions, which is analogous to reduced effective stiffness. However, the statistical behavior of the middle-pinned chain is noticeably different from that of the free chain at short extensions as evident from the poor fit in this regime (right panel, Figure 4).

This effective stiffness change could be manifested in an altered rate of end-to-end juxtaposition or cross-linking. For example, the rate of DNA cyclization or looping reflects the radial distribution function near zero extension. Similarly, one can infer the radial distribution function at larger end-to-end distances from the end-to-end cross-linking rate by using a stiff spacer molecule of fixed length that can link between the ends of the DNA.

Temperature Dependence of Rejection Rate. Middle-pinned chains not only exhibit different statistics than a free wormlike chain but also exhibit counterintuitive temperature dependence. The persistence length is inversely proportional to temperature in the wormlike chain model, and thus higher temperature corresponds to higher flexibilty. In the case of end-pinned chains, the rate of rejection increases as the chain becomes more flexible (Figure 5A). This occurs because more curved conformations will have fewer orientations where they

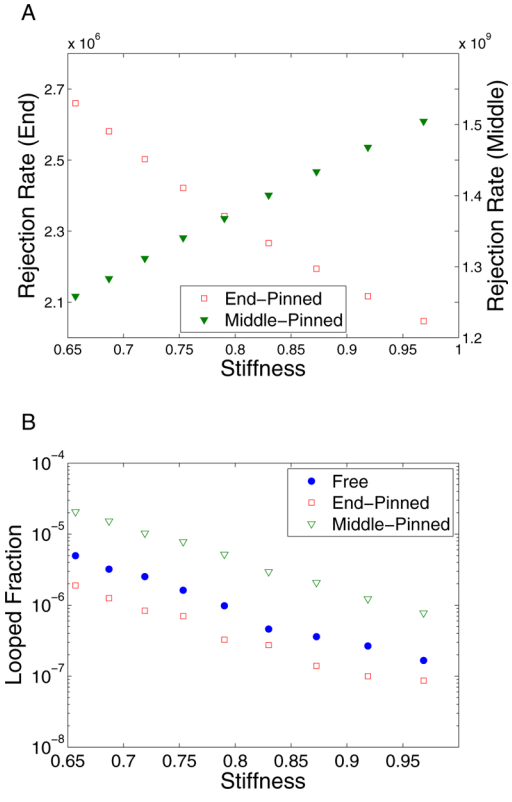

Figure 5. (A) Rejection rate versus stiffness for 186-bp chains. Increasing the stiffness makes rejection less likely for end-pinned chains but more likely for middle-pinned chains. (B) Looping fraction versus stiffness. As the chain becomes stiffer, the looping fraction decreases in all pinning schemes.

dx.doi.org/10.1021/ma4011704 | Macromolecules 2013, 46, 6659–6666

do not intersect the surface relative to straighter conformations. The rate of rejection for the middle-pinned chain, on the other hand, *decreases* as the chain becomes more flexible. This is because while the rate of rejection increases with the curvature of the two halves of the strand on either side of the pinning point, it decreases when the bending angle at the pinning point increases. As the stiffness decreases, the decrease in rejection from sharper bending angles at the pinning point becoming accessible outweighs the increase in rejection due to more curved chains away from the pinning point. Experimentally speaking, one expects surface contact frequency to increase with temperature for an end-pinned chain but decrease for a middle-pinned chain. Nonetheless, in all schemes, decreasing the stiffness has the effect of increasing the looping fraction by lowering the energy of looped conformations (Figure 5B).

This result serves as evidence that the looping behavior of a middle-pinned chain cannot be adequately described by a single effective stiffness parameter $\kappa = L_p/L$. If the number of links increases while the persistence length is held constant, we can expect the rejection rate to increase, whereas if the number of links were held constant while the persistence length decreases, we can expect that rate to decrease. Both changes, however, would have the same effect on the effective stiffness. This result also suggests that global chain statistics of an internally pinned chain would be disproportionately sensitive to changes in the local bending stiffness at the pinning point, which could arise from chemical modification necessary for pinning in real experiments.

Scaling of RMS End-to-End Distance in Different Pinning Schemes. Finally, we present the length dependence of the root-mean-square (RMS) end-to-end distance (r_{RMS}), which best represents the spatial dimension of a chain similar to the radius of gyration. In Figure 6, we show how r_{RMS} varies as a function of length for the three pinning schemes. At very short lengths, r_{RMS} scales linearly with the length of the chain in all cases, as we would expect for a stiff chain. In the semiflexible regime which corresponds to lengths between 100 and 200 bp, r_{RMS} begins to diverge in slope among the different pinning schemes. As we consider longer chains, up to 10^4 bp, r_{RMS} increases with length at a slower rate. At long lengths, we see the same $L^{0.5}$ scaling for all three cases that we would expect for a flexible chain without self-avoidance. However, there is a different constant of proportionality (c) for the different pinning schemes, with the terminally pinned chains on average having a longer r_{RMS} relative to the free case and the middle-pinned chains having a shorter r_{RMS}.

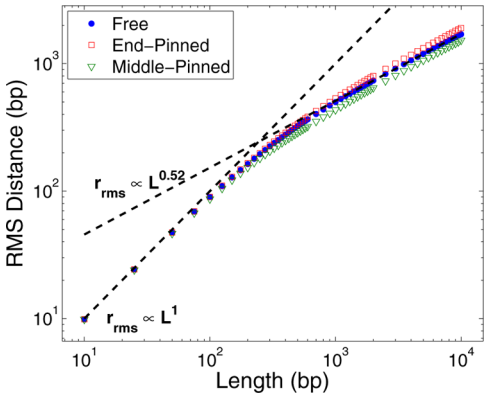

Figure 6. RMS end-to-end distance versus length. At short lengths, the chain does not bend significantly, and the distance scales linearly with length. At long lengths, the behavior approaches that of a random walk chain and scales as $L^{0.52}$. In the flexible limit, we would expect the distance to scale as $L^{0.5}$. The crossover between the stiff regime and the flexible regime occurs between 1× and 2× the persistence length.

The coefficient c in this scaling law ($r_{RMS}^2 = c(2L_pL)$) in the flexible limit can be predicted based on random walk statistics. c is one for an unbound chain. In comparison, it is two for the end-pinned chain in one dimension,[5] which corresponds to 4/3 in three dimensions.[15] For a middle-pinned chain, we calculated c to be $2 - \pi/2$, which corresponds to $4/3 - \pi/6$ in three dimensions (see Supporting Information). These calculated scaling coefficients in different pinning schemes match the difference in r_{RMS} in the flexible limit shown in Figure 6.

Comment on *J* Factor Measurements from an Immobilized DNA. Our results are worthy of discussion in light of surface-based DNA looping experiments that seem to challenge wormlike behavior of dsDNA.[22,23] Ha and Vafabakhsh tethered a dsDNA internally and measured orders of magnitude higher J factor from short dsDNA molecules than predicted.[23] The internal pinning position was about 1/4 the contour length from an end for the short dsDNAs, and therefore their J factor could have been overestimated by a factor of 2 (Figure 1B). In comparison, the J factor that Le and Kim measured from end-pinned dsDNA molecules[22] was higher than the wormlike chain prediction, but by no more than 10-fold. Our simulation suggests that the pinning scheme used could have lowered the J factor by a factor of 2. Regardless, in both experiments, the effect of surface pinning is not strong enough to alter the conclusion that short dsDNA exhibits higher flexibility than predicted. Recently, concern was raised about synthetic DNA used in the former study,[45] but this critique does not apply to the latter study by Le and Kim.[22] Hence, the explanation of frequent looping of dsDNA awaits further investigation.

Outlook. For simplicity, we treated the surface as a hard wall; the potential is a single-variable step function at the boundary. In most single-molecule experiments, however, the surface can be charged[46] and also coated with blocking agents to minimize nonspecific sticking of molecules to the surface.[47] The blocking agents such as poly(ethylene glycol) form a dense entropic cushion that repel molecules away from the surface.[48,49] Hence, the potential from a charged, polymer-grafted surface will be longer-range but softer than the hard wall potential.[50−52] Although the exact surface effect will be complicated to model, we evaluated the effect of a simple surface potential on looping probability using an exponentially decaying function (see Supporting Information). The looping probability of the middle-pinned chain is more strongly affected by the surface than that of the end-pinned chain. The surface also produces opposite effects on the two pinning schemes.

Surface curvature can also influence chain statistics[53] (see Supporting Information), which might have physiological relevance since tethering of DNA to membrane structures occurs inside the cell[54] to regulate gene activity.[55] Reciprocally, semiflexible polymers can change the curvature and bending rigidity of a fluid membrane.[56,57] We also expect that a spatiotemporally fluctuating surface potential can alter chain statistics in a nontrivial way.[58,59]

Further insights into DNA chain statistics in physiological environments might be gained by considering the presence of excluded volume interaction.[60,61] The presence of proteins and higher order structure such as chromatin will also require a

dx.doi.org/10.1021/ma4011704 | *Macromolecules* 2013, 46, 6659−6666

different coarse-graining method.[62,63] Kinetics of end-to-end or internal loop formation[64,65] can also be inferred from the equilibrium probabilty distributions.[66] However, it remains to be determined whether diffusion-limited looping[67] plays a biological role in governing transcriptional noise.[68]

CONCLUSIONS

We studied the statistical behavior of a wormlike chain pinned to a surface using numerical simulation. We focused on the intersection between elastic rod and random walk behaviors. For computational efficiency, we used a Gaussian sampling technique to generate an ensemble of constrained chains that satisfy the boundary conditions. The equilibrium probability distributions of end-to-end distances were constructed from the accepted chain conformations. We have demonstrated that different pinning geometries can enhance or suppress looping behavior in wormlike chain molecules. By fitting a functional form for a free wormlike chain, we showed that the statistics of an end-pinned chain resembles a stiffer unbound chain. The middle-pinned chain behaves like a more flexible chain in some aspects; however, its statistics deviate from an unbound wormlike chain at short end-to-end distances. This in conjuction with the dependence of the acceptance rate on stiffness leads us to conclude the middle-pinned chain cannot be fully characterized by a single parameter for effective stiffness. We also presented scaling laws of mean square end-to-end distance as a function of length in different pinning schemes. We were able to predict the different scaling coefficients observed at large lengths using a random walk model. This work will be important for the analysis of single-molecule experiments that involve surface-tethered polymers and may hold relevance for looping dynamics of DNA in vivo.

ASSOCIATED CONTENT

Supporting Information

Results for wormlike chains confined to spherical shell, looping fraction versus length, and derivation of RMS scaling law for middle-pinned chain. This material is available free of charge via the Internet at http://pubs.acs.org.

AUTHOR INFORMATION

Corresponding Author

*E-mail: harold.kim@physics.gatech.edu (H.D.K.).

Notes

The authors declare no competing financial interest.

ACKNOWLEDGMENTS

The authors acknowledge financial support from Georgia Institute of Technology and the Burroughs Wellcome Fund Career Award at the Scientific Interface. We thank Tung Le for helpful discussions and two anonymous reviewers for their helpful comments and suggestions on the manuscript.

REFERENCES

(1) Pincus, P. *Macromolecules* **1976**, *9*, 386−388.
(2) De Gennes, P. G. *Scaling Concepts in Polymer Physics*; Cornell University Press: Ithaca, NY, 1979.
(3) Gobush, W.; Yamakawa, H.; Stockmayer, W. H.; Magee, W. S. *J. Chem. Phys.* **1972**, *57*, 2839−2843.
(4) Silberberg, A. *J. Phys. Chem.* **1962**, *66*, 1872−1883.
(5) DiMarzio, E. A.; McCrackin, F. L. *J. Chem. Phys.* **1965**, *43*, 539−547.
(6) Roe, R.-J. *Proc. Natl. Acad. Sci. U. S. A.* **1965**, *53*, 50−57.
(7) Motomura, K.; Matuura, R. *J. Chem. Phys.* **1969**, *50*, 1281−1287.
(8) Takahashi, A.; Kawaguchi, M. *Behavior of Macromolecules*; Advances in Polymer Science Vol. *46*; Springer: Berlin, 1982; pp 1−65.
(9) Hehmeyer, O. J.; Arya, G.; Panagiotopoulos, A. Z.; Szleifer, I. *J. Chem. Phys.* **2007**, *126*, 244902−244902-11.
(10) Zhao, B.; Brittain, W. *Prog. Polym. Sci.* **2000**, *25*, 677−710.
(11) Lindberg, E.; Elvingson, C. *J. Chem. Phys.* **2001**, *114*, 6343−6352.
(12) Toral, R.; Chakrabarti, A. *Phys. Rev. E* **1993**, *47*, 4240−4246.
(13) Cifra, P.; Benkova, Z.; Bleha, T. *J. Phys. Chem. B* **2008**, *112*, 1367−1375.
(14) DiMarzio, E. A. *J. Chem. Phys.* **1965**, *42*, 2101−2106.
(15) Eisenriegler, E.; Kremer, K.; Binder, K. *J. Chem. Phys.* **1982**, *77*, 6296−6320.
(16) Slutsky, M. *Am. J. Phys.* **2005**, *73*, 308−314.
(17) Hahn, T. D.; Kovac, J. *Macromolecules* **1990**, *23*, 5153−5154.
(18) Cui, T.; Ding, J.; Chen, J. Z. Y. *Macromolecules* **2006**, *39*, 5540−5545.
(19) Wilhelm, J.; Frey, E. *Phys. Rev. Lett.* **1996**, *77*, 2581−2584.
(20) Czapla, L.; Swigon, D.; Olson, W. K. *J. Chem. Theory Comput.* **2006**, *2*, 685−695.
(21) Towles, K. B.; Beausang, J. F.; Garcia, H. G.; Phillips, R.; Nelson, P. C. *Phys. Biol.* **2009**, *6*, 025001.
(22) Le, T.; Kim, H. *Biophys. J.* **2013**, *104*, 2068−2076.
(23) Vafabakhsh, R.; Ha, T. *Science* **2012**, *337*, 1097−1101.
(24) Cloutier, T. E.; Widom, J. *Mol. Cell* **2004**, *14*, 355−362.
(25) Wiggins, P. A.; Heijden, T. v. d.; Moreno-Herrero, F.; Spakowitz, A.; Phillips, R.; Widom, J.; Dekker, C.; Nelson, P. C. *Nat. Nanotechnol.* **2006**, *1*, 137−141.
(26) Han, L.; Garcia, H. G.; Blumberg, S.; Towles, K. B.; Beausang, J. F.; Nelson, P. C.; Phillips, R. *PLoS One* **2009**, *4*, e5621.
(27) Perez, A.; Lankas, F.; Luque, F. J.; Orozco, M. *Nucleic Acids Res.* **2008**, *36*, 2379−2394.
(28) Skolnick, J.; Fixman, M. *Macromolecules* **1977**, *10*, 944âĂŞ948.
(29) Odijk, T. *J. Polym. Sci., Polym. Phys. Ed.* **1977**, *15*, 477âĂŞ483.
(30) Wenner, J. R.; Williams, M. C.; Rouzina, I.; Bloomfield, V. A. *Biophys. J.* **2002**, *82*, 3160−3169.
(31) Becker, N. B.; Rosa, A.; Everaers, R. *Eur. Phys. J. E* **2010**, *32*, 53−69.
(32) Zhang, Y.; Crothers, D. M. *Biophys. J.* **2003**, *84*, 136−153.
(33) Dickerson, R. E. *Nucleic Acids Res.* **1989**, *17*, 1797−803.
(34) Pérez, A.; Lankas, F.; Luque, F. J.; Orozco, M. *Nucleic Acids Res.* **2008**, *36*, 2379−2394.
(35) Stepanow, S.; Schütz, G. M. *EPL (Europhys. Lett.)* **2002**, *60*, 546.
(36) Mehraeen, S.; Sudhanshu, B.; Koslover, E. F.; Spakowitz, A. J. *Phys. Rev. E* **2008**, *77*, 061803.
(37) Shore, D.; Langowski, J.; Baldwin, R. L. *Proc. Natl. Acad. Sci. U. S. A.* **1981**, *78*, 4833−4837.
(38) Shimada, J.; Yamakawa, H. *Macromolecules* **1984**, *17*, 689−698.
(39) Douarche, N.; Cocco, S. *Phys. Rev. E* **2005**, *72*, 061902.
(40) Allemand, J.-F.; Cocco, S.; Douarche, N.; Lia, G. *Eur. Phys. J. E* **2006**, *19*, 293−302.
(41) Petrov, A. S.; Douglas, S. S.; Harvey, S. C. *J. Phys.: Condens. Matter* **2013**, *25*, 115101.
(42) Daniels, H. E. *Proc. - R. Soc. Edinburgh, Sect. A: Math. Phys. Sci.* **1952**, *63*, 290−311.
(43) Thirumalai, D.; Ha, B.-Y. *Statistical Mechanics of Semiflexible Chains: A Meanfield Variational Approach*; arXiv e-print cond-mat/9705200, 1997.
(44) Winkler, R. G. *J. Chem. Phys.* **2003**, *118*, 2919−2928.
(45) Vologodskii, A.; Frank-Kamenetskii, M. D. *Nucleic Acids Res.* **2013**, PMID: 23677618.
(46) Ambia-Garrido, J.; Vainrub, A.; Pettitt, B. M. *Comput. Phys. Commun.* **2010**, *181*, 2001−2007.
(47) Zanetti-Domingues, L. C.; Martin-Fernandez, M. L.; Needham, S. R.; Rolfe, D. J.; Clarke, D. T. *PLoS One* **2012**, *7*, e45655.
(48) Fang, F.; Satulovsky, J.; Szleifer, I. *Biophys. J.* **2005**, *89*, 1516−1533.

(49) Szleifer, I. *Curr. Opin. Solid State Mater. Sci.* **1997**, *2*, 337−344.
(50) de Gennes, P. G. *Macromolecules* **1980**, *13*, 1069−1075.
(51) Milner, S. T.; Witten, T. A.; Cates, M. E. *Macromolecules* **1988**, *21*, 2610−2619.
(52) Kim, J. U.; Matsen, M. W. *Macromolecules* **2008**, *41*, 246−252.
(53) Park, P. J.; Sung, W. *Phys. Rev. E* **1998**, *57*, 730−734.
(54) Egecioglu, D.; Brickner, J. H. *Curr. Opin. Cell Biol.* **2011**, *23*, 338−345.
(55) Green, E. M.; Jiang, Y.; Joyner, R.; Weis, K. *Mol. Biol. Cell* **2012**, *23*, 1367−1375.
(56) Hiergeist, C.; Lipowsky, R. *J. Phys. II* **1996**, *6*, 1465âĂŞ1481.
(57) Kim, Y. W.; Sung, W. *Phys. Rev. E* **2001**, *63*, 041910.
(58) Shin, J.; Sung, W. *J. Chem. Phys.* **2012**, *136*, 045101−045101−6.
(59) Kim, W. K.; Sung, W. *J. Chem. Phys.* **2012**, *137*, 074903−074903−8.
(60) Toan, N. M.; Marenduzzo, D.; Cook, P. R.; Micheletti, C. *Phys. Rev. Lett.* **2006**, *97*, 178302.
(61) Liu, Z.; Chan, H. S. *J. Chem. Phys.* **2008**, *128*, 145104−145104.
(62) Tokuda, N.; Terada, T. P.; Sasai, M. *Biophys. J.* **2012**, *102*, 296−304.
(63) Koslover, E. F.; Spakowitz, A. J. *Soft Matter* **2013**.
(64) Hyeon, C.; Thirumalai, D. *J. Chem. Phys.* **2006**, *124*, 104905.
(65) Cheng, R. R.; Uzawa, T.; Plaxco, K. W.; Makarov, D. E. *Biophys. J.* **2010**, *99*, 3959−3968.
(66) Afra, R.; Todd, B. A. *J. Chem. Phys.* **2013**, *138*, 174908−174908−8.
(67) Polikanov, Y. S.; Bondarenko, V. A.; Tchernaenko, V.; Jiang, Y. I.; Lutter, L. C.; Vologodskii, A.; Studitsky, V. M. *Biophys. J.* **2007**, *93*, 2726−2731.
(68) Hebenstreit, D. *Trends in Genetics*.